ChemComm

COMMUNICATION

View Article Online
View Journal | View Issue

Cite this: *Chem. Commun.*, 2025, **61**, 2067

Received 19th November 2024,
Accepted 24th December 2024

DOI: 10.1039/d4cc06152g

rsc.li/chemcomm

Towards a long-term stable $MAPbBr_3$ single crystal-based photoconductor with a high on/off ratio and detectivity†

Vishnu Anilkumar, [a] Apurba Mahapatra, *[a] Joanna Kruszyńska, [a] Manoranjan Mandal, [b] Seckin Akin, [c] Pankaj Yadav [d] and Daniel Prochowicz *[a]

Photodetectors based on lead halide perovskites often show excellent performance but poor stability. Herein, we demonstrate a photodetector based on $MAPbBr_3$ single crystals passivated with an ultrathin layer of $PbSO_4$, which shows superior detectivity and on/off ratios compared to the control device due to the combined effect of lower surface traps, reduced recombination and low dark current. In addition, the device retained ~56% of its initial *D with an impressive on/off ratio of ~801 after one year compared to ~22% of *D** and an on/off ratio of ~6 of the control device.**

The extraordinary charge transport capabilities and long carrier diffusion length of lead halide perovskites (LHPs) in the form of single crystals (SCs) have provided clear advantages over their thin film counterparts in recent years.[1,2] Therefore, free-standing LHP SCs have become a suitable platform for the next-generation optoelectronic devices,[3–5] biological image sensors,[6,7] photodetectors (PDs),[1,8,9] X-ray imaging devices[10] and field effect transistors (FETs)[11] due to their excellent detectivity with tuneable bandwidth.[7,12] However, the major shortcomings of the LHP SCs are the formation of high surface trap density during rapid crystallization,[13,14] ion migration[15,16] and low long-term stability under ambient conditions.[17–20] In order to overcome these issues, several strategies have been applied to optimize the optoelectronic properties and stability of LHP SC-based devices.[1,21–24] For example, the addition of ionic liquids or organic ligands to the methylammonium lead bromide ($MAPbBr_3$) precursor solution was found to control the crystallization kinetics for the acquisition of high-quality SCs with a low number of surface and bulk defects.[25–27] As another approach, passivation of the perovskite surface with various agents can simultaneously decrease the surface trap states and reduce ion migration.[28–33] It was reported that the deposition of an ultrathin SnO_x[29] or Al_2O_3[30] layer on top of a perovskite SC effectively passivates surface defects, reduces dark current and improves the stability of the SC against moisture. Stability against moisture and light of LHP SCs could be also improved by applying a polymer-wrapped encapsulation strategy[24] and passivating the crystal surface with hydrophobic compounds.[32] However, it is still necessary to search for a facile method that would not only reduce ion migration, surface traps and dark current of LHP SCs but also enhance their long-term stability under ambient conditions.

Previously, we reported a facile passivation strategy for $MAPbBr_3$ SC with $PbSO_4$, which increases activation energy for ion migration.[33] Here, we analyse the effect of the ultrathin $PbSO_4$ layer on the optoelectronic properties, dark current and photodetection performance of a planar-type $MAPbBr_3$ SC-based PD. The applied surface treatment effectively reduces nonradiative recombination and surface traps, resulting in an improvement in photodetection performance measured under blue light (448 nm). The optimized device exhibited a low dark current of 20.6 nA at 2 V bias, a high detectivity of 1.72×10^{13} Jones and a high on/off ratio of ~2163. Moreover, our passivated PD owing to the hydrophobic nature of $PbSO_4$ exhibited superior long-term ambient stability compared to the control device after one year of aging.

The control $MAPbBr_3$ SCs were synthesized using the previously reported conventional inverse temperature crystallization (ITC) method (see the Experimental section, ESI†).[34] A facile solution-processed dip-coating method was applied to passivate the surface of the $MAPbBr_3$ SC according to our recent work.[33] Specifically, the $MAPbBr_3$ SC was dipped in a 4 mM solution of octylammonium sulfate at various dipping times (10 s, 20 s, 30 s and 40 s). Then, the SC was washed with toluene to remove all unreacted residue species from the surface and dried at 70 °C for 10 min. The SEM images show that the applied

[a] *Institute of Physical Chemistry, Polish Academy of Sciences, Kasprzaka 44/52, 01-224 Warsaw, Poland. E-mail: dprochowicz@ichf.edu.pl, amahapatra@ichf.edu.pl*
[b] *Department of Physics, School of Science, GITAM University, Bengaluru, 561203, India*
[c] *Department of Metallurgical and Materials Engineering, Necmettin Erbakan University, Konya, 42090, Turkey*
[d] *Department of Solar Energy, School of Energy Technology, Pandit Deendayal Energy University, Gandhinagar-382 007, Gujarat, India*

† Electronic supplementary information (ESI) available: Experimental methods and further characterization. See DOI: https://doi.org/10.1039/d4cc06152g

passivation did not affect much the surface of the $MAPbBr_3$ SC (Fig. S1, ESI†). Based on the atomic force microscopy (AFM) analysis, the root mean square (RMS) roughness value of the $MAPbBr_3$ SC reduces significantly after passivation indicating efficient reduction of the vacancy defects (Fig. S2, ESI†). In addition, there is no notable change in the powder XRD pattern of the passivated SC compared to the control $MAPbBr_3$ SC (Fig. S3, ESI†). Using liquid-state ^1H NMR, we confirmed the lack of octylammonium chains on the surface of the $MAPbBr_3$ SC (Fig. S4, ESI†). In turn, the formation of $PbSO_4$ on the surface was confirmed by Fourier transform infrared (FT-IR) transmission measurement, which is consistent with our previous work (Fig. S5, ESI†).[33]

Next, we investigate the effect of surface passivation on the optoelectronic performance of the $MAPbBr_3$ SC-based PD. A thin 100 nm layer of a Pt electrode with 150 μm spacing was deposited on top of the (100) plane forming a photoconductor type PD (for device fabrication, see the Experimental section).[35] The dark current of the pristine and different time-dipped $MAPbBr_3$ SCs is shown in Fig. 1a. In general, the dark current of $MAPbBr_3$ SC-based devices is mainly influenced by the trap density, mobility and conductivity. The dark current reduces with increasing dipping time due to the increasing thickness of as-formed $PbSO_4$ and defect passivation on the crystal surface. The effect of dipping time on the quality of PDs was further verified by analysing the photocurrent under a blue LED light pulse (λ = 448 nm) with the irradiance power densities ranging from 0.1 to 50 mW cm^{-2} at a fixed bias of 2 V (Fig. S6, ESI†). As seen, the photocurrent density (J_{ph}) decreases with increasing dipping time due to the formation of a thicker insulating $PbSO_4$ layer, which restricts the efficient charge transfer, and the maximum J_{ph} was achieved for the device with 20 s dipped $MAPbBr_3$ SC. The logarithmic photocurrent density (J_{ph}) as a function of incident light intensity for each type of PD is shown in Fig. 1b. The highest value of exponent β (fitted with the power law of $J_{ph} \propto P^{\beta}$, where P is the irradiation power and β is the recombination under illumination) for the device with a 20 s dipped $MAPbBr_3$ SC implies the lowest level of recombination compared to the other passivated $MAPbBr_3$ SCs. However, this device shows a slightly higher recombination level compared to the pristine device due to a reduction in conductivity after the passivation. Next, the responsivity (R) and external quantum efficiency (EQE) of the control and passivated SC-based PDs were calculated using eqn (S1) and (S2) (ESI†), respectively (see Supplementary note S1, ESI†). From Fig. 1c and Fig. S7 (ESI†), we can observe that the 20 s dipped $MAPbBr_3$ SC-based PD exhibits almost the same level of R and EQE as compared to the control PD. However, detectivity (D^*) and the I_{on}/I_{off} ratio significantly change for the passivated device (Fig. 1d and e) (for details of calculations, see Supplementary note S1, ESI†). The maximum D^* and I_{on}/I_{off} ratio increase to 1.7 × 10^{13} Jones and 2164 for the 20 s dipped $MAPbBr_3$ SC-based PD compared to 4.9 × 10^{12} Jones and 196 of the control PD under a blue light of 50 mW cm^{-2}, which are among the highest values reported for $MAPbBr_3$ SC based PDs with symmetric electrode contact (Table S1, ESI†). In addition, we investigated the effect of passivation on the trap density (η_{trap}) of the $MAPbBr_3$ SC using the pulsed voltage sweep space charge-limited current (SCLC) method (see the Experimental section note 1, ESI†). To minimize the error in the measurement, we tested four separate controls and the 20 s dipped $MAPbBr_3$ SC. The average surface η_{trap} was found to be 3.31 ± 0.11 × 10^{10} cm^{-3} for the 20 s dipped $MAPbBr_3$ SC, which is almost ~16% lower than that of the control $MAPbBr_3$ SC (3.92 ± 0.14 × 10^{10} cm^{-3}, Fig. S8, ESI†). The steady-state PL spectra of the pristine and passivated $MAPbBr_3$ SCs show an enhancement in PL intensity and blue shift after surface treatment (Fig. S9, ESI†). The enhanced PL intensity and blue shift reconfirm the lower level of nonradiative recombination and passivation of surface traps.[25,28,36] Therefore, the 20 s dipped $MAPbBr_3$ SC-based PD shows comparable performance with superior detectivity and on/off ratio compared to the control PD due to the combined effect of lower surface traps, reduced recombination and low dark current.

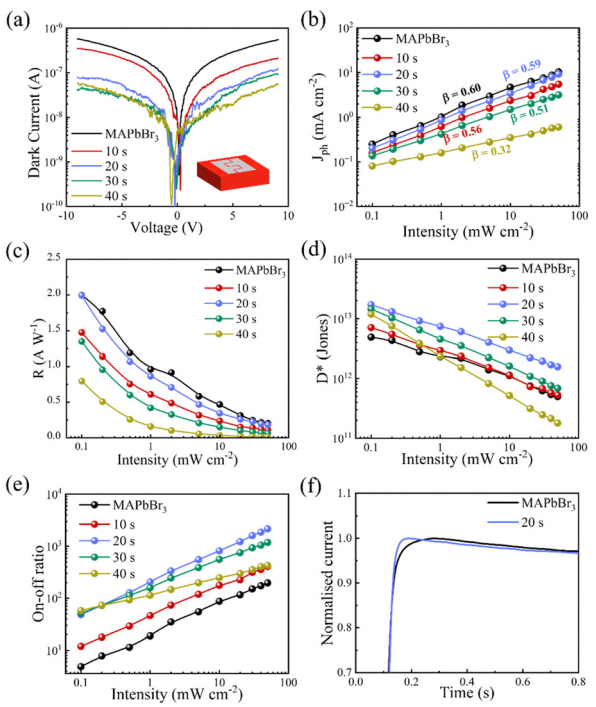

Fig. 1 (a) Dark I–V curve of the pristine $MAPbBr_3$ and passivated SC-based PDs obtained at different dipping times. (b) Photocurrent density (J_{ph}). (c) Responsivity (R), (d) specific detectivity (D^*), and (e) on/off ratio of the pristine and passivated SC-based PDs. (f) Normalized transient photocurrent of the pristine $MAPbBr_3$ and 20 s passivated SC PDs under 1 mW cm^{-2} blue light illumination at 2 V.

Recently, we revealed that ion migration inside the $MAPbBr_3$ SCs is reduced by $PbSO_4$ surface passivation.[33] To further understand the effects of traps and ion migration in control and passivated $MAPbBr_3$ SC-based PDs, we investigated their transient photocurrent decay behaviour under blue light.[33,37] The normalized spectra of the transient photocurrent decay of pristine and 20 s dipped $MAPbBr_3$ SC-based PDs at a 1 mW cm^{-2} irradiance power are shown in Fig. 1f. The time to reach the maximum photocurrent is found to be equal to ~190 ms and ~110 ms for the pristine and 20 s dipped

$MAPbBr_3$ SC based PDs, respectively. The faster photocurrent saturation in the passivated PD is due to the presence of lower trap states.[37] The observed slower photocurrent decay in the 20 s dipped $MAPbBr_3$ SC-based PD indicates a lower level of ion accumulation with time than that of the pristine device due to the lower ion migration of the passivated device.[37] The long-term stability of the $MAPbBr_3$ SC PD under ambient conditions is an essential requirement for the commercialization perspective.[18,19] The formation of an ultrathin and hydrophobic $PbSO_4$ layer on the perovskite surface should improve the stability of the PD by protecting against moisture. To prove it, we exposed both control and 20 s dipped $MAPbBr_3$ SCs (termed as passivated) into water. As shown in Fig. S10 (ESI†), the colour of the passivated $MAPbBr_3$ SC surface slightly changed after 3 s, while the control SC turned into white instantly and decomposed into $PbBr_2$. This experiment confirms that the passivation layer enhances the moisture resistance of the $MAPbBr_3$ SC endowing it with the potential to operate under high moisture conditions. Next, the stability over time was investigated by analysing the changes in the XRD patterns and PL intensity of the pristine and passivated $MAPbBr_3$ SCs (Fig. S11, ESI†). The broadening of the full width at half maxima (FWHM), and a drop in XRD peak intensity in both aged SCs indicate a possible degradation of the crystal quality. On the other hand, a reduction in relative PL intensity with minor Stokes shifts for both aged SCs reveals an increase in trap states and disorder inside the SCs.[38] However, we observed from the XRD pattern of the passivated $MAPbBr_3$ SC that it shows a lower intensity reduction and less peak broadening with a lower PL intensity reduction over time compared to the control SC, indicating its better stability with lower evolution of non-radiative recombination channels.

Furthermore, we measured the long-term shelf-life stability of our PDs under ambient conditions (25 °C, RH = 30 ± 5%) without encapsulation. Both control and passivated $MAPbBr_3$ SC-based PDs show a notable increment of I_{ph} during their initial aging process (Fig. 2a). This could be attributed to the initial formation of hydrogen bonds between the uncoordinated Br atoms and water molecules on the surface, which suppresses nonradiative recombination by localizing photoexcited electrons to the perovskite/water interface.[20] This localization of photoexcited electrons helps to reduce the electron–hole overlay concentration on the surface and increases the excited-state lifetime of the $MAPbBr_3$ SC.[17]

Remarkably, over one year, the passivated $MAPbBr_3$ SC-based PD shows only ~12% reduction in I_{ph} compared to ~19% photocurrent reduction of the control device. Fig. S12 (ESI†) shows the dark current at 2 V bias as a function of aging time, and both the PDs showed a noticeable increment in J_d over the aging time. It is well known that the $MAPbBr_3$ SC is ionic in nature and the ion migration leads to the formation of ionic vacancies with aging time. On the other hand, exposure to the oxygen and moisture can degrade the surface quality of the $MAPbBr_3$ SC leading to the formation of higher defects and trap states with increasing aging time. These defects can lower the activation energy for leakage current and/or act as charge carriers triggering a higher dark current with aging time for both the PDs. As shown in Fig. 2b, the dark current densities (J_d) with increasing rate are calculated using eqn (S5) (see Supplementary note S1, ESI†). As expected, the passivated $MAPbBr_3$ SC-based PD exhibits

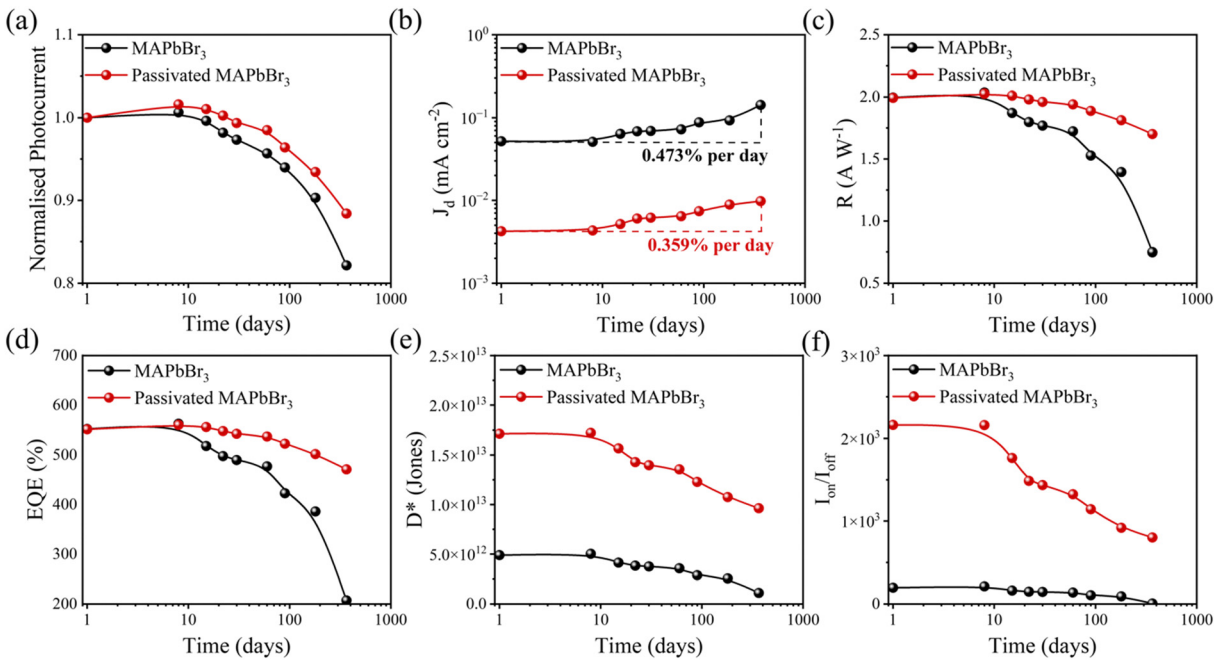

Fig. 2 Time-dependent (a) normalized photocurrent; (b) dark current density (J_{ph}), (c) responsivity (R), (d) EQE, and (e) specific detectivity (D^*) of the control and 20 s dipped $MAPbBr_3$ SC-based PDs under a blue light of 0.1 mW cm^{-2}. (f) Time-dependent on/off ratio of the control and 20 s passivated $MAPbBr_3$ SC-based PDs under a blue light of 50 mW cm^{-2}.

a lower rate of change in J_d per day (0.359%) compared to the control PD (0.473% per day) due to suppression of ion migration and enhanced moisture resistance by the passivation layer. Next, we calculated the PD performance metrics including responsivity (R), specific detectivity (D^*), EQE, and the on/off ratio as a function of aging time (Fig. 2c–f). As seen, maximum R and EQE reduce to 1.7 A W^{-1} and 470% for the passivated $MAPbBr_3$ SC based PD, and are almost two times higher than the respective values of the control PD (0.96 A W^{-1} and 267%) under a blue light of 0.1 mW cm^{-2} after a period of one year. There is evident negative effect of the aging time on the values of D^* and the on/off ratio for the both PDs due to the inverse correlation with the dark current. The control PD retains only ~22% of its initial D^*, while the passivated $MAPbBr_3$ SC-based PD maintains ~56% of its initial D^* after one year. Interestingly, the passivated $MAPbBr_3$ SC-based PD can maintain a higher level of D^* (9.63×10^{12} Jones) and on/off (~801) ratio after one year compared to the freshly prepared control $MAPbBr_3$ SC-based PD.

In conclusion, we have demonstrated that the surface treatment of the $MAPbBr_3$ SC with $PbSO_4$ can be an efficient strategy to achieve efficient and highly stable photoconductor type devices. The optimized passivated $MAPbBr_3$ SC-based PD shows a maximum D^* of 1.7×10^{13} Jones and a high I_{on}/I_{off} ratio of 2164. In addition, the $PbSO_4$ passivation layer not only protects the device against moisture but also reduces surface traps and ion migration in the device. As a result, the passivated $MAPbBr_3$ SC-based PD exhibits robust stability under ambient conditions for more than one year and maintains a high level of D^* (9.63×10^{12}) and on/off (~801) ratio. Our study reveals that the ultrathin hydrophobic $PbSO_4$ layer on the $MAPbBr_3$ SC surface can not only improve the detectivity of the PD but can also enhance its long-term operational stability under ambient conditions, which can open a path for its further commercialization and practical applications.

The authors acknowledge the National Science Centre (Grant OPUS-20, No. 2020/39/B/ST5/01497) for financial support.

Data availability

Data for this article are available at RepOD at **https://doi.org/10.18150/8Q6FX4**.

Conflicts of interest

There are no conflicts to declare.

Notes and references

1 Y. Zhang, Y. Liu and S. (Frank) Liu, *Adv. Funct. Mater.*, 2023, **33**, 2210335.
2 S. Trivedi, D. Prochowicz, N. Parikh, A. Mahapatra, M. K. Pandey, A. Kalam, M. M. Tavakoli and P. Yadav, *ACS Omega*, 2021, **6**, 1030–1042.
3 Y. He, M. Petryk, Z. Liu, D. G. Chica, I. Hadar, C. Leak, W. Ke, I. Spanopoulos, W. Lin, D. Y. Chung, B. W. Wessels, Z. He and M. G. Kanatzidis, *Nat. Photonics*, 2021, **15**, 36–42.
4 L. Zhao, Y. Zhou, Z. Shi, Z. Ni, M. Wang, Y. Liu and J. Huang, *Nat. Photonics*, 2023, **17**, 315–323.
5 L. Zhao, Z. Shi, Y. Zhou, X. Wang, Y. Xian, Y. Dong, O. Reid, Z. Ni, M. C. Beard, Y. Yan and J. Huang, *Nat. Photonics*, 2024, **18**, 250–257.
6 Q. Wang, G. Zhang, H. Zhang, Y. Duan, Z. Yin and Y. Huang, *Adv. Funct. Mater.*, 2021, **31**, 2100857.
7 L. Li, S. Ye, J. Qu, F. Zhou, J. Song and G. Shen, *Small*, 2021, **17**, 2005606.
8 V. Anilkumar, A. Mahapatra, J. Nawrocki, R. D. Chavan, P. Yadav and D. Prochowicz, *Adv. Opt. Mater.*, 2024, **12**, 2302032.
9 Y. Ma, W. Guo, Q. Fan, H. Xu, L. Tang, Y. Liu, W. Li, X. Liu, J. Luo and Z. Sun, *Adv. Funct. Mater.*, 2023, **33**, 2210235.
10 Z. Zhang, H. Li, H. Di, D. Liu, W. Jiang, J. Ren, Z. Fan, F. Liao, L. Lei, G. Li, Y. Xiong and Y. Zhao, *ACS Appl. Electron. Mater.*, 2023, **5**, 388–396.
11 W. Yu, F. Li, L. Yu, M. R. Niazi, Y. Zou, D. Corzo, A. Basu, C. Ma, S. Dey, M. L. Tietze, U. Buttner, X. Wang, Z. Wang, M. N. Hedhili, C. Guo, T. Wu and A. Amassian, *Nat. Commun.*, 2018, **9**, 5354.
12 Z. Li, T. Yan and X. Fang, *Nat. Rev. Mater.*, 2023, **8**, 587–603.
13 B. Murali, E. Yengel, C. Yang, W. Peng, E. Alarousu, O. M. Bakr and O. F. Mohammed, *ACS Energy Lett.*, 2017, **2**, 846–856.
14 C. Geng, Y. Feng, Q. Chen, Y. Jiang, S. M. H. Qaid and M. Yuan, *J. Phys. Chem. C*, 2023, **127**, 17617–17623.
15 W. Peng, C. Aranda, O. M. Bakr, G. Garcia-Belmonte, J. Bisquert and A. Guerrero, *ACS Energy Lett.*, 2018, **3**, 1477–1481.
16 M. García-Batlle, J. Mayén Guillén, M. Chapran, O. Baussens, J. Zaccaro, J.-M. Verilhac, E. Gros-Daillon, A. Guerrero, O. Almora and G. Garcia-Belmonte, *ACS Energy Lett.*, 2022, **7**, 946–951.
17 R. Long, W. Fang and O. V. Prezhdo, *J. Phys. Chem. Lett.*, 2016, **7**, 3215–3222.
18 C. Wang, B. R. Ecker, H. Wei, J. Huang and Y. Gao, *J. Phys. Chem. C*, 2018, **122**, 3513–3522.
19 J. I. J. Choi, M. E. Khan, Z. Hawash, K. J. Kim, H. Lee, L. K. Ono, Y. Qi, Y.-H. Kim and J. Y. Park, *J. Mater. Chem. A*, 2019, **7**, 20760–20766.
20 Z. Song, N. Shrestha, S. C. Watthage, G. K. Liyanage, Z. S. Almutawah, R. H. Ahangharnejhad, A. B. Phillips, R. J. Ellingson and M. J. Heben, *J. Phys. Chem. Lett.*, 2018, **9**, 6312–6320.
21 P. K. Nayak, D. T. Moore, B. Wenger, S. Nayak, A. A. Haghighirad, A. Fineberg, N. K. Noel, O. G. Reid, G. Rumbles, P. Kukura, K. A. Vincent and H. J. Snaith, *Nat. Commun.*, 2016, **7**, 13303.
22 J. Zhou and J. Huang, *Adv. Sci.*, 2018, **5**, 1700256.
23 W. Zia, C. A. Aranda, J. Pospisil, A. Kovalenko, M. Rai, C. Momblona, S. Gorji, G. Muñoz-Matutano and M. Saliba, *Chem. Mater.*, 2023, **35**, 5458–5467.
24 Y. Zhu, Y. Liu, B. Jin, Y. Shi, Z. Wu, J. Cao, H. Li and C. Wu, *Macromol. Mater. Eng.*, 2022, **307**, 2200452.
25 A. Mahapatra, V. Anilkumar, J. Kruszyńska, N. Mrkyvkova, P. Siffalovic, P. Yadav and D. Prochowicz, *J. Mater. Chem. C*, 2024, **12**, 2953–2960.
26 M. K. Kim, Y. S. Choi, D. Kim, K. Heo, S. J. Oh, S. Lee, J. An, H. Yoo, S. H. Kim, T.-S. Kim and B. Shin, *ACS Appl. Mater. Interfaces*, 2023, **15**, 57404–57414.
27 Y. Liu, X. Zheng, Y. Fang, Y. Zhou, Z. Ni, X. Xiao, S. Chen and J. Huang, *Nat. Commun.*, 2021, **12**, 1686.
28 L. Chen, H. Wang, W. Zhang, F. Li, Z. Wang, X. Wang, Y. Shao and J. Shao, *ACS Appl. Mater. Interfaces*, 2022, **14**, 10917–10926.
29 Y. Chai, J. Jiang, L. Wu, Z. Sun, S. Fang, L. Shen and K. Yao, *J. Phys. Chem. Lett.*, 2024, **15**, 3859–3865.
30 X.-D. Wang, Y.-H. Huang, J.-F. Liao, Z.-F. Wei, W.-G. Li, Y.-F. Xu, H.-Y. Chen and D.-B. Kuang, *Nat. Commun.*, 2021, **12**, 1202.
31 W. Zhang, H. Wang, H. Dong, F. Li, Z. Wang and Y. Shao, *J. Mater. Chem. C*, 2022, **10**, 17353–17363.
32 K. Wang, B. Ecker, M. Li, J. Huang and Y. Gao, *J. Phys. Chem. C*, 2023, **127**, 19599–19606.
33 A. Mahapatra, N. Parikh, H. Kumari, M. K. Pandey, M. Kumar, D. Prochowicz, A. Kalam, M. M. Tavakoli and P. Yadav, *J. Appl. Phys.*, 2020, **127**, 185501.
34 Y. Cho, H. R. Jung, Y. S. Kim, Y. Kim, J. Park, S. Yoon, Y. Lee, M. Cheon, S. Jeong and W. Jo, *Nanoscale*, 2021, **13**, 8275–8282.
35 A. Mahapatra, V. Anilkumar, R. D. Chavan, P. Yadav and D. Prochowicz, *ACS Photonics*, 2023, **10**, 1424–1433.
36 S. Yang, S. Chen, E. Mosconi, Y. Fang, X. Xiao, C. Wang, Y. Zhou, Z. Yu, J. Zhao, Y. Gao, F. De Angelis and J. Huang, *Science*, 2019, **365**, 473–478.
37 A. Mahapatra, V. Anilkumar, J. Nawrocki, S. V. Pandey, R. D. Chavan, P. Yadav and D. Prochowicz, *Adv. Electron. Mater.*, 2023, **9**, 2300226.
38 A. Mahapatra, D. Prochowicz, J. Kruszyńska, S. Satapathi, S. Akin, H. Kumari, P. Kumar, Z. Fazel, M. Mahdi Tavakoli and P. Yadav, *J. Mater. Chem. C*, 2021, **9**, 15189–15200.

